Highlights

- Ion beam sputter-deposition was used to produce thin films from the system FeCrMnNi.
- Two thin films were obtained at same deposition conditions.
- The high-entropy alloy thin film exhibited grains with sizes around 100 – 200 nm.
- The non-equiatomic thin film exhibited grains with sizes around of 40 nm.
- High-entropy alloy and nucleation theories are used to reflect on the results.

Synthesis and characterisation of high-entropy alloy thin films as candidates for coating nuclear fuel cladding alloys

Matheus A. Tunes, Vladimir M. Vishnyakov and Stephen E. Donnelly

School of Computing and Engineering
University of Huddersfield
Queensgate, HD1 3DH
Huddersfield – United Kingdom

Abstract

Thin films of the quaternary system FeCrMnNi were synthesised by ion beam sputter-deposition. The films were deposited on a silicon substrate at approximately 350 K. A high-entropy alloy thin film (HEATF) and a non-equiatomic thin film were obtained. Energy Dispersive X-Ray Spectroscopy (EDX) and Transmission Electron Microscopy (TEM) were used to determine thin film composition and the atomic structure. The non-equiatomic thin film exhibited a polycrystalline structure with nanometre-sized. Microstructural analysis of the HEATF, which had close to equimolar composition, showed large crystals and planar defects. The microstructural differences between the HEATF and the non-equiatomic thin film are discussed in terms of current high-entropy alloy theory, previous work on thin films and nucleation theory.

Keywords: Ion-beam sputter-deposition; High entropy alloys; Transmission electron microscopy; Energy dispersive X-ray spectroscopy; Accident Tolerant Fuels

INTRODUCTION

Thin film technology is a successful branch of materials science and metallurgy having numerous applications in surface treatments aimed at enhancing a wide variety of material properties such as mechanical strength, heat, wear, frictional and scratch resistance as well as reducing corrosion and oxidation in many metals [1]. The diversity and enormous potential of this technology have supported the progress of many scientific areas by means of coating functional materials used in applications that include optics [2,3], steel tools [4,5], space technology [6], computer chips and microelectronics [7,8], medicine [9] and the nuclear industry [10–14].

In the loss-of-coolant accident at the Fukushima-Daiichi complex in 2011, fuel rods made of a zirconium alloy were subjected to high-temperatures and underwent catastrophic oxidation producing H gas that leading to the core meltdown [15]. As a result, the nuclear community has recently initiated efforts to investigate new accident tolerant fuel (ATF) systems aiming at preventing and mitigating possible deleterious effects in structural nuclear materials under severe conditions [15,16]. One particular approach has been to coat zirconium alloys with hard thin films such as nitrides [17,18] and carbides [11,19]. Such ceramics are well known for their excellent corrosion resistance [20], chemical inertness [21,22] and reduced H pickup [23], however, their applicability is diminished in some cases where low ductility, reduced heat transfer rate and crack resistance are regarded as essential.

Parallel to the progress of the ATF program, recent scientific investigations in the field of high-entropy alloys (HEA) have led to the possibility of designing new metallic alloys with superior metallurgical stability at room and high temperatures, improved radiation resistance and better corrosion behaviour when compared to conventional cladding alloys such as Zircaloys and stainless steels [24–29]. HEAs are a new class of alloy with four or more elements in equiatomic composition [24,30]. This condition results in minimisation of the Gibbs free energy as the configurational entropy is maximised. This results in a material with superior phase stability, which enables HEAs to withstand significant doses of irradiation without accumulation of damage and degradation of their properties. To assess the radiation hardness, ion irradiation has been applied to several different HEAs and the most recent results have demonstrated evidence of self-healing effects in some of these systems [31–33]. The multicomponent nature makes it difficult to model such materials and predict their behaviour. Both modelling and experimental data are needed to shape our understanding of these alloys. The first papers on thin film HEA deposition used HEAs as target materials in

reactive sputtering under a N atmosphere [34,35]. Pure metallic coatings were deposited later [36,37]. The possibility to adjust the elemental content and to alter material properties provides the possibility of tailoring properties to applications [38,39].

In this work, we report the synthesis of multicomponent materials based on the quaternary system FeCrMnNi, which at close to equiatomic (e.g. equimolar) composition can be regarded as a HEATF. The technique of ion beam sputter-deposition was employed in order to produce the thin films. Transmission Electron Microscopy (TEM) characterisation has revealed significant differences in the microstructure when the composition is far from equiatomic and when the film is in quasi-equiatomic composition. Given the metallic nature of the material, its potential high radiation hardness and oxidation resistance [39], the HEATF can be regarded as a metallic coating candidate within the scope of ATF research programs.

MATERIALS AND METHODS

Thin films were synthesised using the ion beam sputter-deposition technique from elemental targets of Fe, Cr, Mn and Ni. An ion source producing 1.25 keV Ar ions was used to sputter the elements onto a Si substrate (Fig.1). The substrate is not intentionally heated in this work, but mainly due to radiation heating from the targets, the substrate temperature during the 2h deposition rises to the region of 350 – 370 K. Base vacuum in the deposition chamber was 1.5×10^{-4} Pa and during deposition the pressure in the chamber was at around 3×10^{-2} Pa. The deposition time was the same for both thin films (120 min) discussed in this paper. A HEATF and a non-equiatomic thin film are presented in this work, produced under the same envelope of deposition conditions. Elemental targets under sputter ion beam were geometrically adjusted in order to achieve the non-equiatomic and equiatomic compositions. The elemental composition of the thin films is then directly related to the geometric configuration of the sputtering targets. The close to equiatomic composition was reached under a specific geometric configuration after several trial and error attempts.

The compositions were then determined using an Oxford EDX system in an FEI Quanta 3D FEG Scanning Electron Microscope (SEM). Atomic compositions of the HEATF and the non-equiatomic thin film are listed in table 1. The standardless quantification method with ZAF correction [40] was used in order to estimate the composition from the X-ray analysis. Set of various electron energies (30, 20 and 15 keV) and measurements at different spots were also used to reduce uncertainties. Uncertainties for the composition were estimated to be approximately 4-5% of the measured values after extended acquisition time

and standard optimisation and quantification algorithms provided by the manufacturer. Conventional Focused Ion-Beam (FIB) lift-out technique [41] was used to produce TEM samples that were further analysed in a JEOL 3010 TEM operating at 300 kV.

RESULTS

Figure 2(a) shows a TEM lamella attached to a Mo grid. The lamella has a top layer protection of Pt and it was welded onto a TEM grid with carbon deposition. After multiple measurements with cross-sectional SEM micrographs, it was concluded that the non-equiatomic thin film has 1.51±0.06 µm thickness, while the HEATF has thickness of 1.58±0.05 µm. Therefore, the deposition rate was roughly the same for both thin films at 0.013 nm/min.

The microstructure of the non-equiatomic thin film is presented in figure 3. Figure 3(a) shows a BFTEM image at focus. Nanocrystallites are observed throughout the microstructure with sizes around of 5 nm and 50 nm. The nanocrystalline structure was confirmed with the selected-area electron diffraction (SAED) pattern exhibited in the figure 3(b).

Another BFTEM micrograph of a different region of the TEM lamella and at a higher magnification (40k), figure 4a, shows the nanocrystallites in further detail and by defocusing the electron beam, surface roughening can be seen as "speckled" Fresnel contrast. The roughening was also observed in the HEATF to some degree as shown in figure 4b.

Figure 5a-i is a set of BFTEM micrographs of the non-equiatomic thin film. When tilting around the x-axis within the TEM holder, diffraction contrast in the bright field image served to identify some of the individual grains in each case. It was thus possible to conclude that the microstructure is composed entirely of nanocrystals with sizes around of 40 nm. Figure 6a is tracing of all the grains visible in the micrographs at the different tilt angles that were presented in figure 5. The area in which the analysis was carried out is represented by the dashed-rectangle in the figure 5a. The dark-field TEM image (DFTEM) figures 6b and 6c also show the grain structure visible at 0º and 10º, respectively.

With respect to the HEATF, figure 7a features a BFTEM micrograph at focus. For this case, the SAED analysis (7b-c) showed that the HEATF microstructure is composed of grains with sizes varying from 100 to 200 nm. The DFTEM micrograph, figure 7d, clearly demonstrates much bigger grain size compared with the non-equiatomic thin film. Crystallographic analysis carried out with the diffraction pattern has confirmed that the

single-crystals are of face-centred cubic (FCC) structure. The microstructure of the HEATF has also revealed the presence of planar defects similar to twinning (fig. 7a).

DISCUSSION

(a) The dynamics of nucleation and the Gibbs free energy

The microstructural differences between the HEATF and the non-equiatomic thin film can be discussed using current HEA theory. It has been established that the maximum configurational entropy in a metallurgical system is reached when the alloying elements are mixed in equal amounts [42]. Despite the fact that in a thermodynamic system the mixing entropy is subdivided into four different types, e.g. configurational, vibrational, magnetic dipole and electronic randomness, Fultz [43] concluded that the configurational contribution is the dominant part of the mixing entropy. In terms of statistical mechanics, this can be expressed using the classical Boltzmann entropy theory which states that for N different alloying elements, the general form of the entropy of mixing is:

$$\Delta S = -k_B N_a \sum_{i=1}^{N} x_i \ln x_i \qquad (1)$$

Where k_B and N_a are Boltzmann's constant and Avogadro's number, respectively and the variable x_i corresponds to the molar fraction of each alloying element present in the system with the boundary condition of $\sum_{i=1}^{N} x_i = 1$. Thus, in equation (1), the maximum configurational entropy is a condition where the all the alloying elements N have equimolar fractions implying that the Gibbs free energy will be minimum (equation 2) as the entropy overcomes the contribution of the enthalpy. The condition of minimum also holds for the temperature range to which the alloy may be subjected: as the higher T, the lower is the ΔG.

$$\Delta G = \Delta H - T\Delta S \qquad (2)$$

Due to their equiatomic nature**,** the HEAs possess major features that establish a new category of metallic alloy. The high-entropy effect favours the formation of a single-phase solid solution instead of the clustering of atoms or the precipitation of secondary phases in the microstructure as this would reduce the configurational entropy [42,44].

In the case of the non-equiatomic thin film, the TEM microstructural analysis showed the presence of nanocrystallites whilst the grains in the HEATF case have grown under the same deposition conditions. Comparing the diffraction patterns of the non-equiatomic thin film with the HEATF, the latter case resembles a typical crystalline pattern. For the non-equiatomic thin film, the diffraction pattern is of a nanocrystalline alloy (grain-sizes smaller

than 100 nm according to the definition proposed by Jang [45]). The diffraction patterns are consistent with the grain-size analysis carried out in the TEM as showed in the figures 6 and 7. The major difference between the two thin films is that in the HEATF the grains are bigger. With respect to the FCC crystal structure observed for the HEATF, the results are in agreement with previous works in the literature for the same HEA system [46,47].

Differences in composition were found to be influential in the final microstructures: both morphology and crystal structure indicate that for the HEATF, the grains started to nucleate and grow at the early stages of deposition while in the non-equiatomic case, although the nucleation rate was higher, the formation of smaller crystals was due to suppressed growth kinetics. As studied by Hollomon and Turnbull [48,49], the Gibbs free energy of a material plays a major role in the formation of *embryos* which affect the overall nucleation kinetics. The authors reported an inversely proportional relationship between the Gibbs free energy and the critical radius for nucleation: as the HEATF has a lower Gibbs free energy than the non-equiatomic thin film, in the latter case the critical radius for an *embryo* in the heterogeneous nucleation is smaller. We speculate that in the HEATF, the high-entropy effect may act in favour of a uniform nucleation rate for the most stable phase in the given equiatomic composition, although the configurational entropy for the non-equiatomic thin film and the HEATF are very similar when equation (1) is used: $1.32k_BN_a$ and $1.38k_BN_a$, respectively. These observations are in agreement with previously reported results on thin solid films [50], but further studies are needed in order to better understand the nucleation kinetics of HEA thin films as the current lack of experimental data in equiatomic alloy systems, such as latent heat and surface energy, poses challenges for deeper analytical calculations. Additionally, the influence of configurational entropy, regarded as the most influential component of the high-entropy effect, should be investigated in greater depth as small differences in calculated entropies were observed to be significant in the final microstructures of the synthesised thin films in this work.

It is worth emphasising that both the temperature of the substrate and the deposition conditions were equal for the two thin films: ~ 350 K (probably equal to $0.2T_m$, T_m= 1685 K for Si [51]). As studied by Thornton [52], for substrate temperatures within the range of 0.3 – $0.5T_m$, surface mobility is sufficiently high to promote grain boundary migration and even recrystallisation. While the deposition temperature reported in this work is outside of this region, some ion assistance by ions backscattered from the targets during the film growth will promote the surface mobility of solute atoms. The nucleation but lack of growth of grains in

the non-equiatomic thin film is probably rather a feature of the non-equiatomic condition which affects the overall nucleation kinetics rather than due to lack of atomic diffusion [53].

(b) Surface roughening and planar defects

Another difference between the HEATF and the non-equiatomic thin film lies in the observation of planar defects in the first case, although as a recent subject of research some authors have reported such defects in nanocrystalline materials [45,54,55]. In both thin films, surface roughening was also observed in underfocused micrographs (figure 4a and 4b). As studied previously by Roitburd [56], the ion beam sputter-deposition of a thin film on a substrate induces the generation of residual stresses that can be the cause of deposition-related effects such as thermal expansion mismatch, epitaxy and phase transitions. It has been shown that these stresses can be a significant fraction of the shear modulus [57]. Dislocation motion, cracking, surface roughening, twinning and stacking faults are some possible mechanisms by which the residual stresses are relieved [7,56].

The whole-solute matrix in the HEATF is a multicomponent solid solution formed from elemental targets with slightly different atomic sizes [47]. This atomic size difference creates a "severe distorted lattice" that was confirmed using X-ray diffraction analysis (XRD): the distorted Miller planes generates X-ray peak a with decreased intensity [24]. The observation of planar defects throughout the microstructure of the HEATF may indicate that they are being formed in order to reduce the elastic strain energy mismatch by the mixing of the different kind of solute atoms in equimolar proportion in combination with the residual stresses induced by the deposition method, but these facts highlight the need for further research to evaluate the impact of planar defects in both the tribological and mechanical properties of the HEATFs.

CONCLUSIONS

Metallic alloys with nanometre-sized grains have attracted the attention of the materials science community due to their superior properties for a wide range of applications. Recently, ongoing investigations in high-entropy alloys have already established a new paradigm [28,29] for materials applications at high temperatures with increased mechanical strength. These superior properties of HEAs are commonly attributed to the thermodynamic stability of the single-phase crystal structure at equiatomic compositions.

In this work, we have demonstrated the viability of producing nanocrystalline thin films using ion beam sputter-deposition from elemental targets of Fe, Cr, Mn and Ni. Two

thin films were produced under the same deposition conditions: a non-equiatomic thin film and a HEATF. The TEM analysis revealed that in the HEATF, the thin film at close equiatomic composition, the grains have grown significantly and their sizes were on the order of 100 – 200 nm. Conversely, in the far from equimolar composition, the thin film exhibits nanocrystals whose growth has been less then those in the HEATF. Differences in the composition and in the Gibbs free energy states were used to discuss the observed results regarding the evolution of the microstructures.

Owing to the potential high radiation hardness of the high-entropy alloy systems, its potential high corrosion resistance and metallic nature [32], we propose the FeCrMnNi HEA in thin film form as a candidate material for future research within the scope of accident tolerant nuclear fuel systems. Further work is needed to investigate the properties of such HEATFs particularly those relevant to nuclear environments such as corrosion behaviour, mechanical resistance and compatibility with nuclear fuel cladding alloys.

ACKNOWLEDGEMENTS

The authors are grateful to the Engineering and Physical Sciences Research Council (EPRSC) for funding the MIAMI-1 (grant number EP/E017266/1) and MIAMI-II (EP/M028283/1) facilities.

LIST OF REFERENCES

[1] M. Wittmer, H. Melchior, Applications of TiN thin films in silicon device technology, Thin Solid Films. 93 (1982) 397–405. doi:10.1016/0040-6090(82)90145-6.
[2] K.L. Chopra, I. Kaur, Thin Films in Optics, in: Thin Film Device Appl., Springer US, Boston, MA, 1983: pp. 55–88. doi:10.1007/978-1-4613-3682-2_2.
[3] D.E. Aspnes, Optical properties of thin films, Thin Solid Films. 89 (1982) 249–262. doi:10.1016/0040-6090(82)90590-9.
[4] Y.H. Yoo, D.P. Le, J.G. Kim, S.K. Kim, P. Van Vinh, Corrosion behavior of TiN, TiAlN, TiAlSiN thin films deposited on tool steel in the 3.5 wt.% NaCl solution, Thin Solid Films. 516 (2008) 3544–3548. doi:10.1016/j.tsf.2007.08.069.
[5] R. Buhl, H.K. Pulker, E. Moll, TiN coatings on steel, Thin Solid Films. 80 (1981) 265–270. doi:10.1016/0040-6090(81)90233-9.
[6] C.M. Lew, R. Cai, Y. Yan, Zeolite Thin Films: From Computer Chips to Space Stations, Acc. Chem. Res. 43 (2010) 210–219. doi:10.1021/ar900146w.
[7] M. Ohring, Materials Science of Thin Films, Second Edition, Academic Press, 2001. doi:10.1016/B978-0-12-524975-1.50018-5.
[8] M. Kamalasanan, S. Chandra, Sol-gel synthesis of ZnO thin films, Thin Solid Films. 288 (1996) 112–115. doi:10.1016/S0040-6090(96)08864-5.
[9] R.J. Narayan, Nanostructured diamondlike carbon thin films for medical applications, Mater. Sci. Eng. C. 25 (2005) 405–416. doi:10.1016/j.msec.2005.01.026.
[10] B.R. Maier, B.L. Garcia-Diaz, B. Hauch, L.C. Olson, R.L. Sindelar, K. Sridharan,

Cold spray deposition of Ti2AlC coatings for improved nuclear fuel cladding, J. Nucl. Mater. 466 (2015) 712–717. doi:10.1016/j.jnucmat.2015.06.028.
[11] Y. Katoh, G. Vasudevamurthy, T. Nozawa, L.L. Snead, Properties of zirconium carbide for nuclear fuel applications, J. Nucl. Mater. 441 (2013) 718–742. doi:10.1016/j.jnucmat.2013.05.037.
[12] M.F. Beaufort, M. Vallet, J. Nicola, E. Oliviero, J.F. Barbot, In-situ evolution of helium bubbles in SiC under irradiation, J. Appl. Phys. 118 (2015). doi:10.1063/1.4936562.
[13] Y. Katoh, H. Kishimoto, A. Kohyama, The influences of irradiation temperature and helium production on the dimensional stability of silicon carbide, J. Nucl. Mater. 307 (2002) 1221–1226. doi:10.1016/S0022-3115(02)01062-0.
[14] Y. Katoh, L.L. Snead, I. Szlufarska, W.J. Weber, Radiation effects in SiC for nuclear structural applications, Curr. Opin. Solid State Mater. Sci. 16 (2012) 143–152. doi:10.1016/j.cossms.2012.03.005.
[15] S.J. Zinkle, K.A. Terrani, J.C. Gehin, L.J. Ott, L.L. Snead, Accident tolerant fuels for LWRs: A perspective, J. Nucl. Mater. 448 (2014) 374–379. doi:10.1016/j.jnucmat.2013.12.005.
[16] N.M. George, K. Terrani, J. Powers, A. Worrall, I. Maldonado, Neutronic analysis of candidate accident-tolerant cladding concepts in pressurized water reactors, Ann. Nucl. Energy. 75 (2015) 703–712. doi:10.1016/j.anucene.2014.09.005.
[17] E. Alat, A.T. Motta, R.J. Comstock, J.M. Partezana, D.E. Wolfe, Ceramic coating for corrosion (c3) resistance of nuclear fuel cladding, Surf. Coatings Technol. 281 (2015) 133–143. doi:10.1016/j.surfcoat.2015.08.062.
[18] E. Alat, A.T. Motta, R.J. Comstock, J.M. Partezana, D.E. Wolfe, Multilayer (TiN, TiAlN) ceramic coatings for nuclear fuel cladding, J. Nucl. Mater. 478 (2016) 236–244. doi:10.1016/j.jnucmat.2016.05.021.
[19] L. Hallstadius, S. Johnson, E. Lahoda, Cladding for high performance fuel, Prog. Nucl. Energy. 57 (2012) 71–76. doi:10.1016/j.pnucene.2011.10.008.
[20] M. Zhou, Y. Makino, M. Nose, K. Nogi, Phase transition and properties of Ti–Al–N thin films prepared by r.f.-plasma assisted magnetron sputtering, Thin Solid Films. 339 (1999) 203–208. doi:10.1016/S0040-6090(98)01364-9.
[21] F. Khatkhatay, L. Jiao, J. Jian, W. Zhang, Z. Jiao, J. Gan, H. Zhang, X. Zhang, H. Wang, Superior corrosion resistance properties of TiN-based coatings on Zircaloy tubes in supercritical water, J. Nucl. Mater. 451 (2014) 346–351. doi:10.1016/j.jnucmat.2014.04.010.
[22] S. PalDey, S.C. Deevi, Properties of single layer and gradient (Ti,Al)N coatings, Mater. Sci. Eng. A. 361 (2003) 1–8. doi:10.1016/S0921-5093(03)00473-8.
[23] S.J. Zinkle, G.S. Was, Materials challenges in nuclear energy, Acta Mater. 61 (2013) 735–758. doi:10.1016/j.actamat.2012.11.004.
[24] B.S. Murty, J.-W. Yeh, S. Ranganathan, High-entropy alloys, Butterworth-Heinemann, 2014.
[25] Y. Zhang, T.T. Zuo, Z. Tang, M.C. Gao, K.A. Dahmen, P.K. Liaw, Z.P. Lu, Microstructures and properties of high-entropy alloys, Prog. Mater. Sci. 61 (2014) 1–93. doi:10.1016/j.pmatsci.2013.10.001.
[26] D. Raabe, C.C. Tasan, H. Springer, M. Bausch, From high-entropy alloys to high-entropy steels, Steel Res. Int. 86 (2015) 1127–1138. doi:10.1002/srin.201500133.
[27] T. Nagase, P.D. Rack, J.H. Noh, T. Egami, In-situ TEM observation of structural changes in nano-crystalline CoCrCuFeNi multicomponent high-entropy alloy (HEA) under fast electron irradiation by high voltage electron microscopy (HVEM), Intermetallics. 59 (2015) 32–42. doi:10.1016/j.intermet.2014.12.007.

[28] Y. Zou, J.M. Wheeler, H. Ma, P. Okle, R. Spolenak, Nanocrystalline High-Entropy Alloys: A New Paradigm in High-Temperature Strength and Stability, Nano Lett. 17 (2017) 1569–1574. doi:10.1021/acs.nanolett.6b04716.
[29] C.C. Koch, Nanocrystalline high-entropy alloys, J. Mater. Res. 32 (2017) 3435–3444. doi:10.1557/jmr.2017.341.
[30] J.-W. Yeh, Physical Metallurgy of High-Entropy Alloys, JOM. 67 (2015) 2254–2261. doi:10.1007/s11837-015-1583-5.
[31] F. Granberg, K. Nordlund, M.W. Ullah, K. Jin, C. Lu, H. Bei, L.M. Wang, F. Djurabekova, W.J. Weber, Y. Zhang, Mechanism of radiation damage reduction in equiatomic multicomponent single phase alloys, Phys. Rev. Lett. 116 (2016) 135504. doi:10.1103/PhysRevLett.116.135504.
[32] C. Lu, L. Niu, N. Chen, K. Jin, T. Yang, P. Xiu, Y. Zhang, F. Gao, H. Bei, S. Shi, M.-R. He, I.M. Robertson, W.J. Weber, L. Wang, Enhancing radiation tolerance by controlling defect mobility and migration pathways in multicomponent single-phase alloys, Nat. Commun. 7 (2016) 13564. doi:10.1038/ncomms13564.
[33] M.W. Ullah, D.S. Aidhy, Y. Zhang, W.J. Weber, Damage accumulation in ion-irradiated Ni-based concentrated solid-solution alloys, Acta Mater. 109 (2016). doi:10.1016/j.actamat.2016.02.048.
[34] T.K. Chen, T.T. Shun, J.W. Yeh, M.S. Wong, Nanostructured nitride films of multi-element high-entropy alloys by reactive DC sputtering, Surf. Coatings Technol. 188–189 (2004) 193–200. doi:10.1016/j.surfcoat.2004.08.023.
[35] V. Dolique, A.-L. Thomann, P. Brault, Y. Tessier, P. Gillon, Complex structure/composition relationship in thin films of AlCoCrCuFeNi high entropy alloy, Mater. Chem. Phys. 117 (2009) 142–147. doi:10.1016/j.matchemphys.2009.05.025.
[36] V. Dolique, A.-L. Thomann, P. Brault, Y. Tessier, P. Gillon, Thermal stability of AlCoCrCuFeNi high entropy alloy thin films studied by in-situ XRD analysis, Surf. Coatings Technol. 204 (2010) 1989–1992. doi:10.1016/j.surfcoat.2009.12.006.
[37] B.R. Braeckman, D. Depla, Structure formation and properties of sputter deposited Nb x -CoCrCuFeNi high entropy alloy thin films, J. Alloys Compd. 646 (2015) 810–815. doi:10.1016/j.jallcom.2015.06.097.
[38] A. Marshal, K.G.G. Pradeep, D. Music, S. Zaefferer, P.S.S. De, J.M.M. Schneider, Combinatorial synthesis of high entropy alloys: Introduction of a novel, single phase, body-centered-cubic FeMnCoCrAl solid solution, J. Alloys Compd. 691 (2017) 683–689. doi:10.1016/j.jallcom.2016.08.326.
[39] G.R. Holcomb, J. Tylczak, C. Carney, Oxidation of CoCrFeMnNi High Entropy Alloys, JOM. 67 (2015) 2326–2339. doi:10.1007/s11837-015-1517-2.
[40] J. Trincavelli, S. Limandri, R. Bonetto, Standardless quantification methods in electron probe microanalysis, Spectrochim. Acta - Part B At. Spectrosc. 101 (2014) 76–85. doi:10.1016/j.sab.2014.07.016.
[41] S. Nakahara, Recent development in a TEM specimen preparation technique using FIB for semiconductor devices, Surf. Coatings Technol. 169–170 (2003) 721–727. doi:10.1016/S0257-8972(03)00206-8.
[42] H.K.D.H. Bhadeshia, High entropy alloys, Mater. Sci. Technol. 31 (2015) 1139–1141. doi:10.1179/0267083615Z.000000000969.
[43] B. Fultz, Vibrational thermodynamics of materials, Prog. Mater. Sci. 55 (2010) 247–352. doi:10.1016/j.pmatsci.2009.05.002.
[44] B. Cantor, Stable and metastable multicomponent alloys, Ann. Chim. Sci. Des Matériaux. 32 (2007) 245–256. doi:10.3166/acsm.32.245-256.
[45] D. Jang, Nano-sized Nanocrystalline and Nano-twinned Metals, in: B. Bhushan (Ed.), Encycl. Nanotechnol., Springer Netherlands, Dordrecht, 2012: pp. 1739–1747.

doi:10.1007/978-90-481-9751-4_385.
[46] Y.F.F. Ye, Q. Wang, J. Lu, C.T.T. Liu, Y. Yang, High-entropy alloy: challenges and prospects, Mater. Today. 19 (2016) 349–362. doi:10.1016/j.mattod.2015.11.026.
[47] N.A.P.K. Kumar, C. Li, K.J. Leonard, H. Bei, S.J. Zinkle, Microstructural stability and mechanical behavior of FeNiMnCr high entropy alloy under ion irradiation, Acta Mater. 113 (2016) 230–244. doi:10.1016/j.actamat.2016.05.007.
[48] J.H. Hollomon, D. Turnbull, Nucleation, Prog. Met. Phys. 4 (1953) 333–388. doi:10.1016/0502-8205(53)90020-3.
[49] R.W. Cahn, P. Haasen, Physical Metallurgy, North-Holland, 1992. doi:10.1016/B978-0-444-89875-3.
[50] J.A. Venables, G.D.T. Spiller, M. Hanbucken, Nucleation and growth of thin films, Reports Prog. Phys. 47 (1984) 399–459. doi:10.1088/0034-4885/47/4/002.
[51] E.P. Donovan, F. Spaepen, D. Turnbull, J.M. Poate, D.C. Jacobson, Heat of crystallization and melting point of amorphous silicon, Appl. Phys. Lett. 42 (1983) 698–700. doi:10.1063/1.94077.
[52] J.A. Thornton, Influence of apparatus geometry and deposition conditions on the structure and topography of thick sputtered coatings, J. Vac. Sci. Technol. 11 (1974) 666–670. doi:10.1116/1.1312732.
[53] M. Birkholz, B. Selle, W. Fuhs, S. Christiansen, H. Strunk, R. Reich, Amorphous-crystalline phase transition during the growth of thin films: The case of microcrystalline silicon, Phys. Rev. B. 64 (2001) 1–9. doi:10.1103/PhysRevB.64.085402.
[54] Q. An, W.A. Goddard, K.Y. Xie, G.D. Sim, K.J. Hemker, T. Munhollon, M. Fatih Toksoy, R.A. Haber, Superstrength through Nanotwinning, Nano Lett. 16 (2016) 7573–7579. doi:10.1021/acs.nanolett.6b03414.
[55] J.R. Greer, Nanotwinned metals: It's all about imperfections, Nat. Mater. 12 (2013) 689–690. doi:10.1038/nmat3721.
[56] A.L. Roitburd, Equilibrium structure of epitaxial layers, Phys. Status Solidi. 37 (1976) 329–339. doi:10.1002/pssa.2210370141.
[57] N. Sridhar, J.M. Rickman, D.J. Srolovitz, Twinning in thin films—II. Equilibrium microstructures, Acta Mater. 44 (1996) 4097–4113. doi:10.1016/S1359-6454(96)00059-6.

LIST OF TABLES

FIGURE CAPTIONS

Figure 1: The ion beam sputter-deposition system.

Figure 2: SEM micrograph showing the HEATF TEM lamella attached to a TEM grid.

Figure 3: The nanostructure of the non-equiatomic thin films. Figure 3 (a) is a BFTEM micrograph at focus. The SAED pattern from the area indicated by the circle in figure 3a is shown in figure 3b.

Figure 4: BFTEM underfocused micrographs (a) of the non-equiatomic thin film and (b) the HEATF showing surface roughening as evidenced by the speckled contrast. The defocus degree was of –0.95 μm for both images. The scale marker in (a) also applies to (b).

Figure 5: BFTEM images of the non-equiatomic thin film from 0º to 10º x-axis tilt. The dashed rectangle in (a) is the area analysed to compose figure 6a.

Figure 6: (a) The nanocrystalline composite image showing the grain pattern for the images from 0º to 10º of x-axis tilting. DFTEM micrographs for (b) 0º and (c) 10º of tilting.

Figure 7: TEM characterisation of the HEATF. Figure (a) is a focused BFTEM image. Figure 7(b) is the diffraction pattern corresponding to 7(a) and (d) exhibits the dark-field image of the studied region.

TABLES

Table 1: Elemental composition of the synthesised thin films.		
Element	**Composition [at. %]**	
	Non-equiatomic thin film	**HEATF**
Fe	14.6±0.7	23.7±1.1
Cr	21.7±1.1	22.9±1.3
Mn	39.3±2.0	25.8±1.2
Ni	24.4±1.2	27.6±1.4

Figure 01

Click here to download Figures (if any): Fig01.pdf

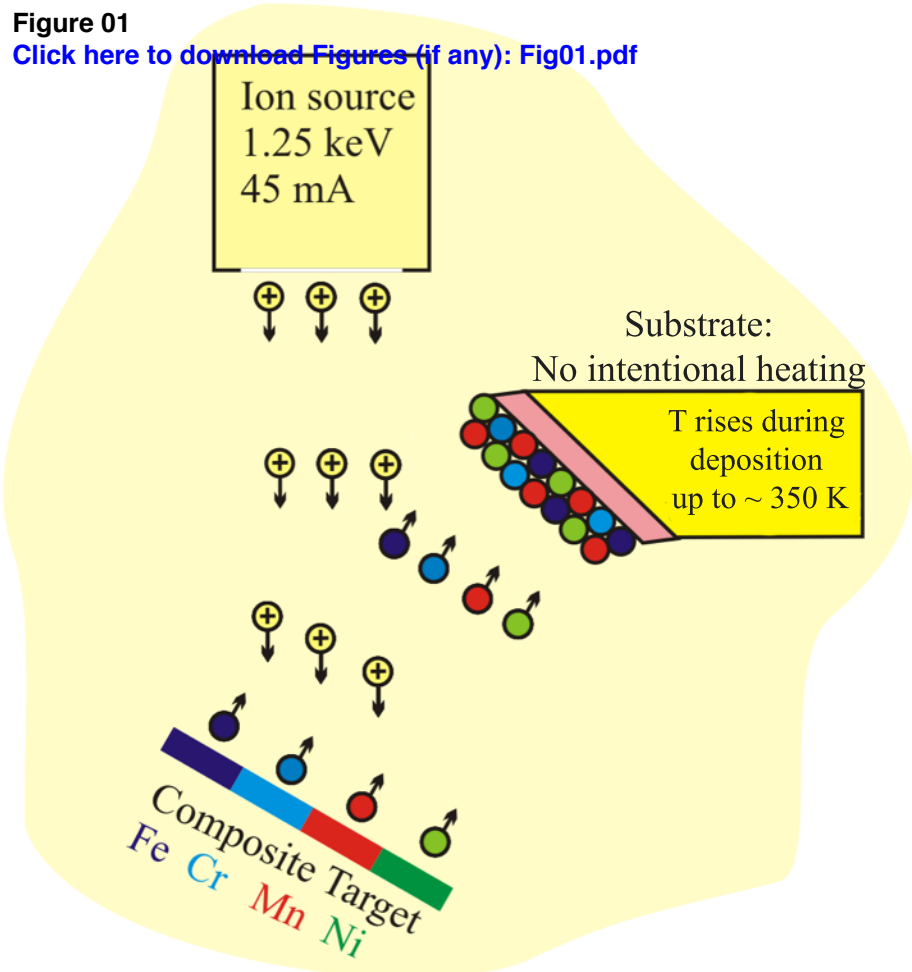

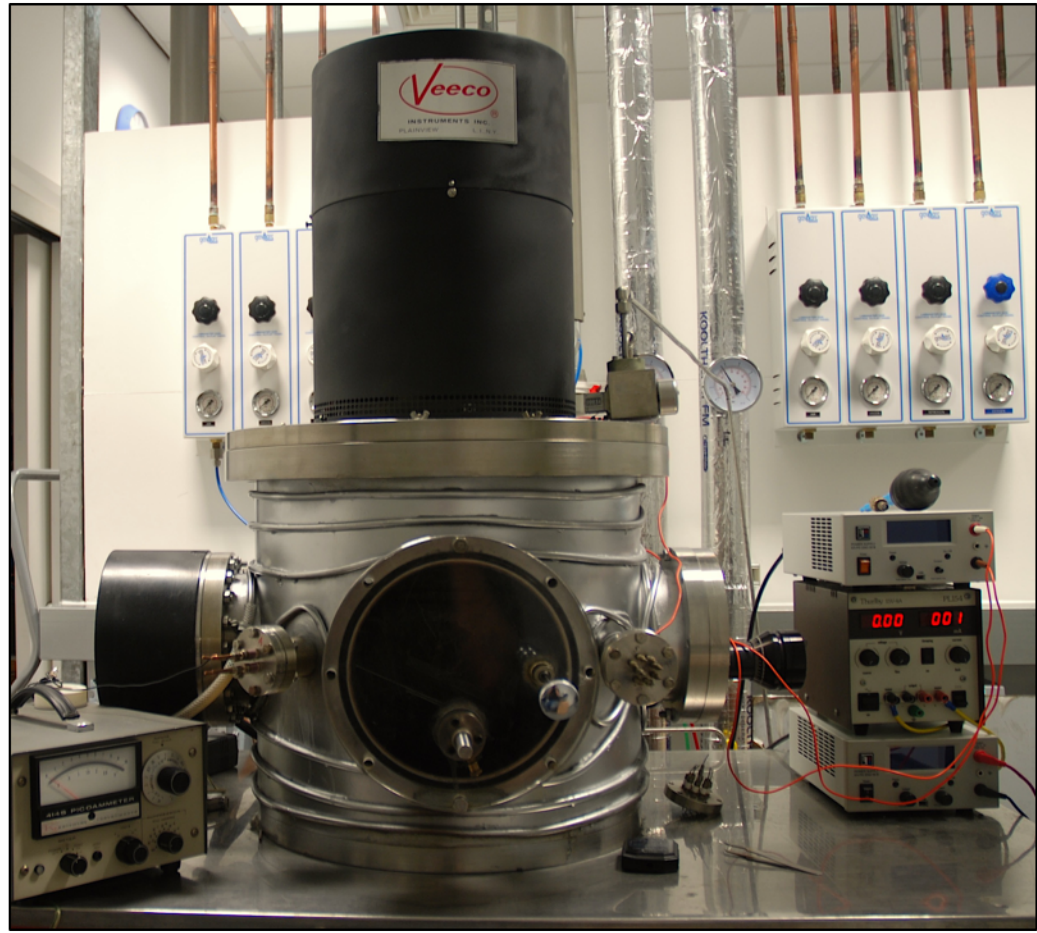

Figure 02

Click here to download Figures (if any): Fig02.pdf

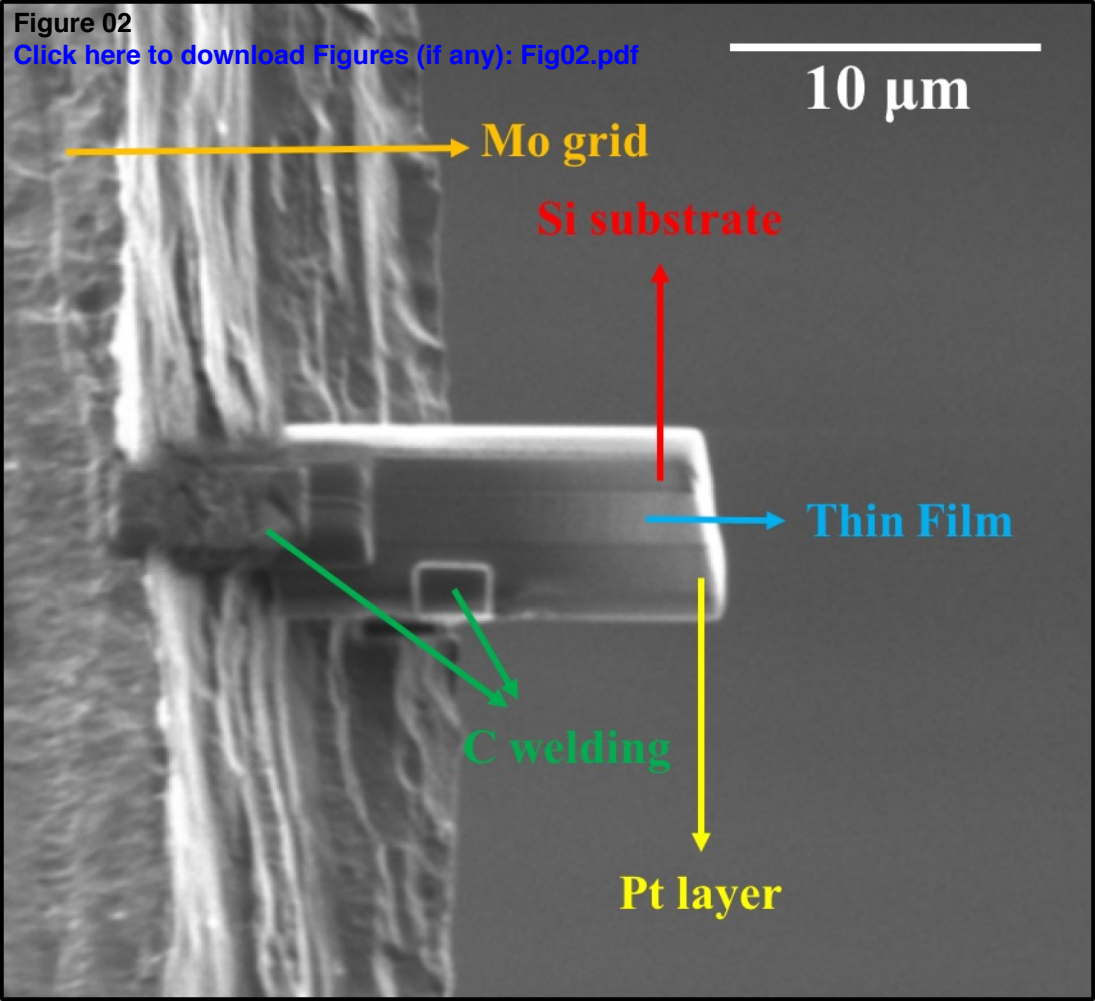

Figure 03

Click here to download Figures (if any): Fig03.pdf

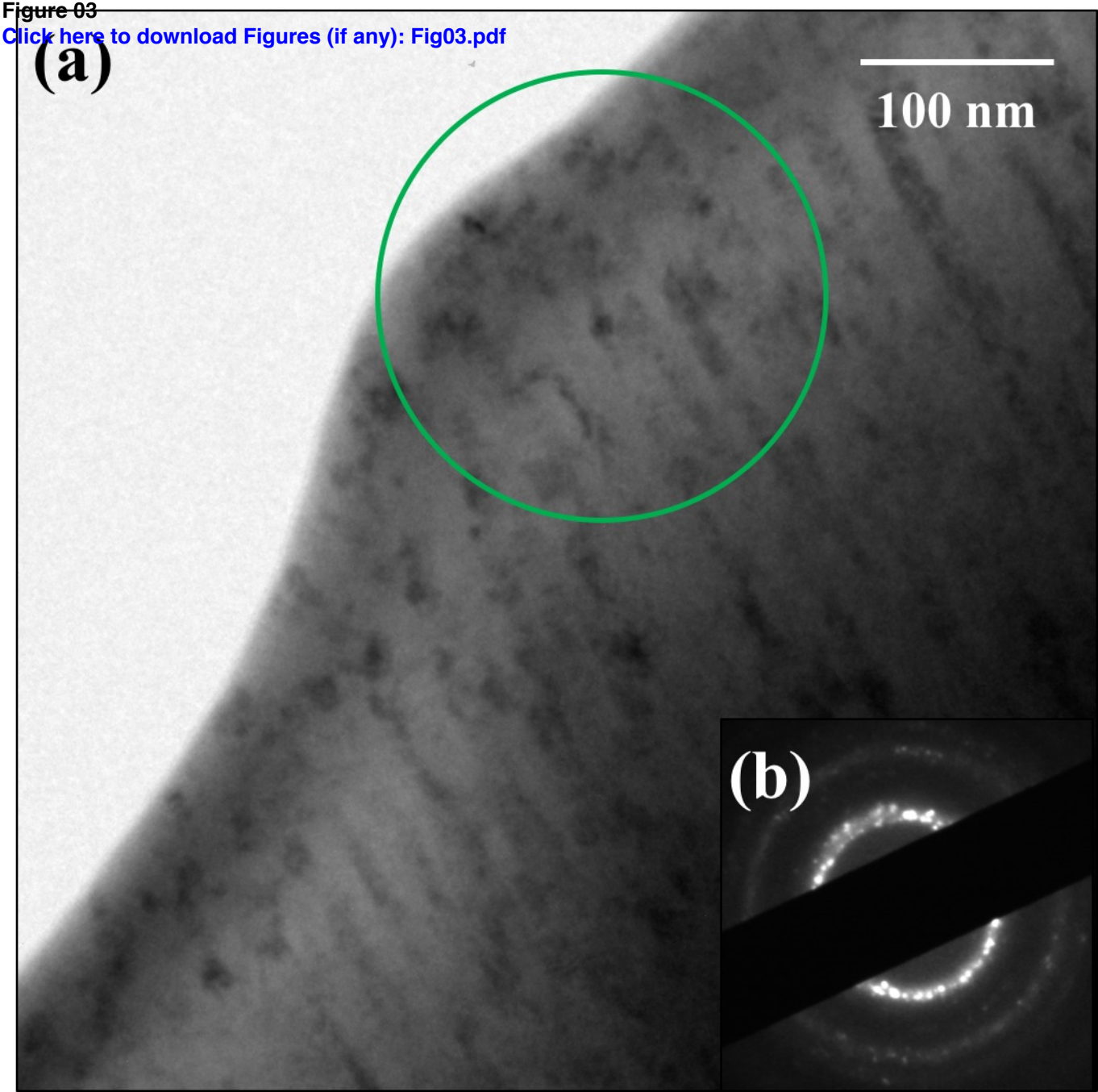

Figure 04
Click here to download Figures (if any): Fig04.pdf

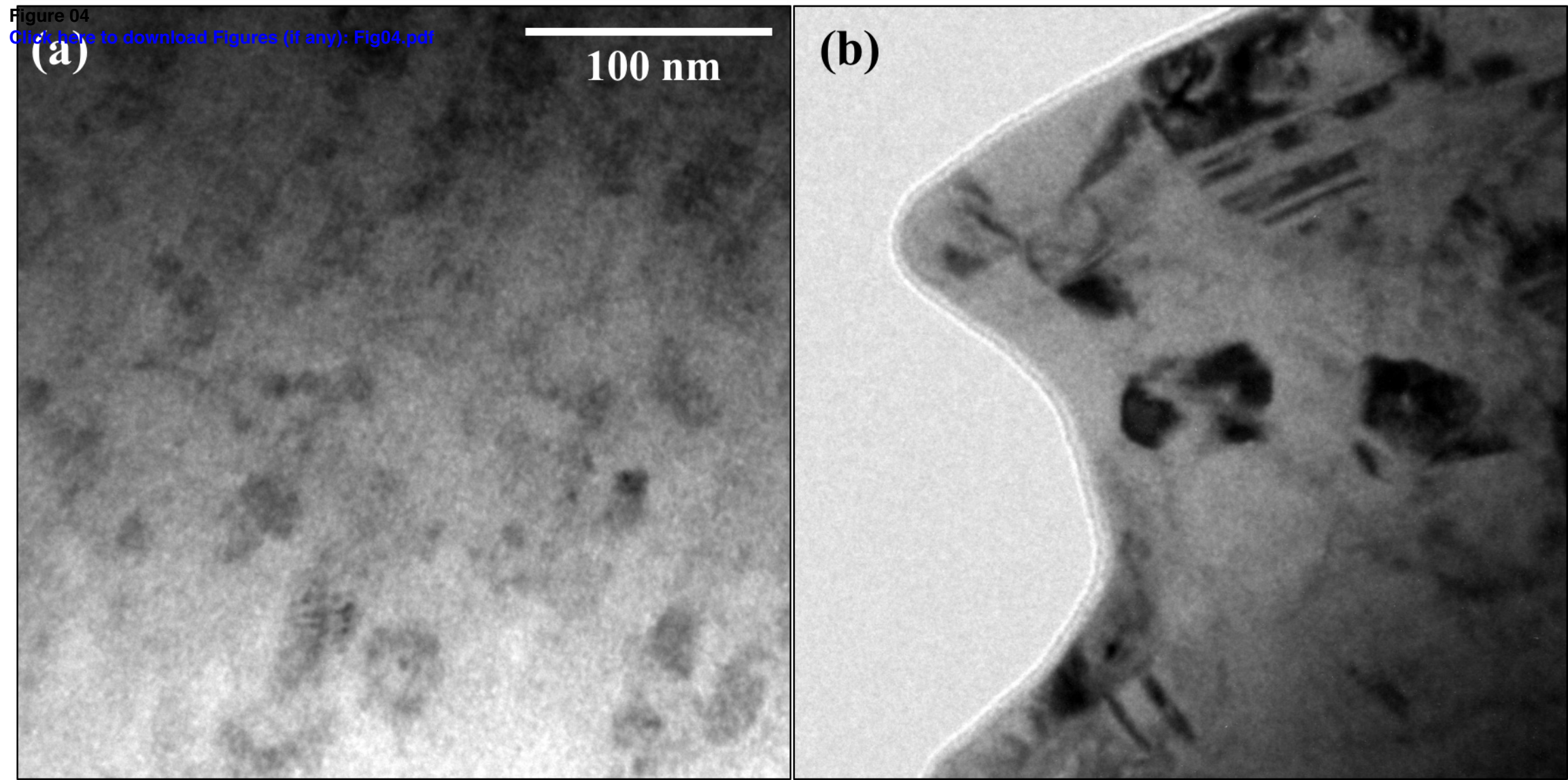

Figure 05
Click here to download Figures (if any): Fig05.pdf

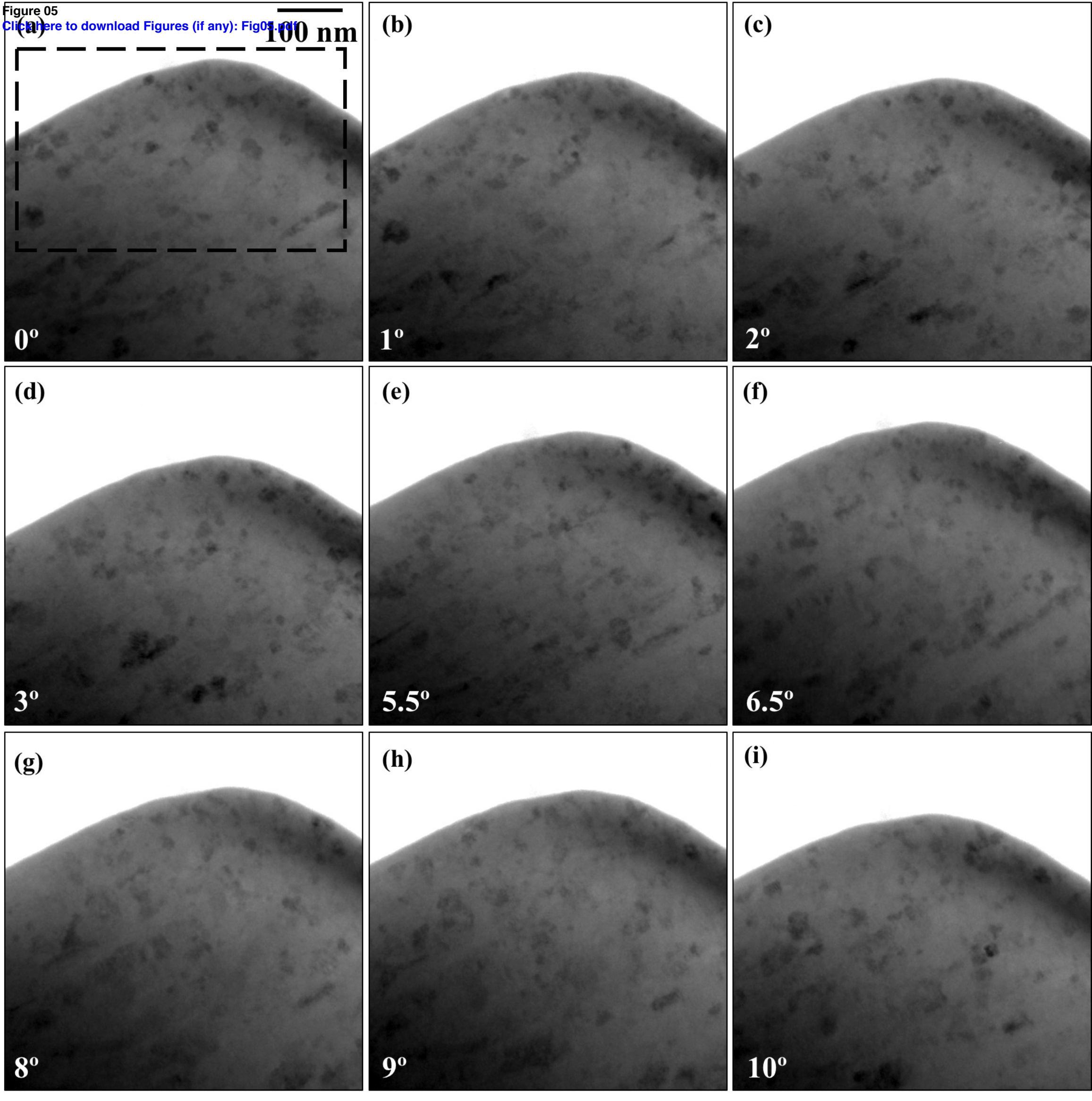

Figure 06

Click here to download Figures (if any): Fig06.pdf

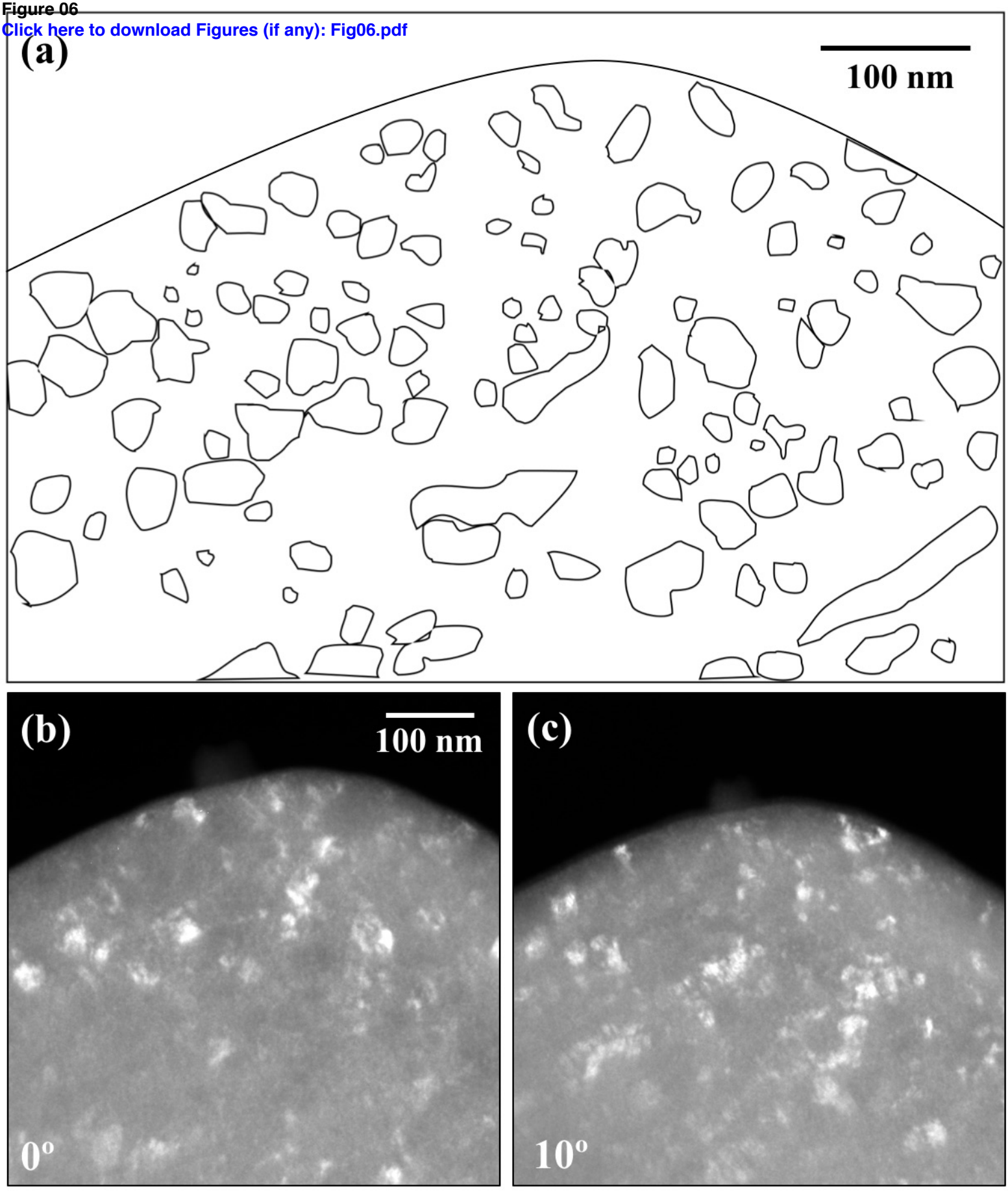

Figure 07

Click here to download Figures (if any): Fig07.pdf